Validation of the satellite-based landfast ice mapping

Master Thesis

Msc Programme 'Applied Polar and Marine Science POMOR'

State University of St. Petersburg, Russia

University of Hamburg

by Valeria Selyuzhenok

St. Petersburg, 2011

-

Contents

Glossary **6**

1 Introduction **7**

1.1 Overview 7

1.2 Satellite based fast ice detection methods 9

1.3 Aim of this work 10

2 Data and methods **11**

2.1 AMSR-E data 11

2.2 Fast ice retrieval method 13

2.3 Validation dataset 18

2.4 Pattern of seasonal fast ice development in the southeastern Laptev Sea 19

3 Results **21**

3.1 Assessment of the accuracy of the algorithm 21

3.2 Impact of changing Δ *days* parameter 21

3.3 Impact of changing *time span* parameter 23

3.4 Impact of changing *block size* parameter 23

3.5 Impact of changing *threshold* parameter 24

4 Discussion **25**

5 Conclusion **28**

Acknowledgement **29**

References **30**

Abstract

Supervisors:

Prof. Dr. R. Gerdes, Alfred Wegener Institute for Polar and Marine Research, Germany

Dr. E. Shalina, St. Petersburg State University, Faculty of Geography and Geoecology, Russia

Landfast sea ice is distinctive feature of Arctic and Antarctic coastal zones. It is contiguous with the shore and relatively immobile ice cover that has fastened along the coast or to the sea floor. The role of landfast ice in the climate system was highlighted in numerous studies. However for most of the marginal seas of the Arctic Ocean information on the seasonal variability and extent of the fast ice are not existent or strongly limited in time and space. Recent studies revealed that deficient representation of fast ice in coupled sea ice-ocean models affects the accuracy of the modeled processes. A permanent consideration of fast ice in coupled sea ice-ocean models requires an automatic procedure to derive fast ice extent for the entire Arctic at a reasonable spatial and temporal resolution. This study presents an investigation of a method for automatic fast ice mapping by means of passive microwave satellite data. Commonly used for fast ice detection correlation technique was performed on Advanced Microwave Scanning Radiometer (AMSR-E) brightness temperature data with spatial resolution 6.25 km. The method was implemented for southeastern Laptev Sea. Different settings were applied to produce fast ice maps for the region in order to investigate the sensitivity of the presented method. Also the derived fast ice maps were compared with high resolution ASAR data. Validation reveals that the method is capable to reproduce enormous changes in the fast ice extent and map fast ice edge accurately. However, some seasonal limitations for the method application occur.

List of Figures

1 Fast ice extent for April 2010 (adopted from AARI, 2010). 8

2 AMSR-E/Aqua daily average brightness temperatures from 89 GHz channel, vertically polarized. Grey colour indicates missing data. 12

3 The flowchart shows steps of fast ice mapping. The letters refer to the kind of data obtained after each step. 14

4 Calculation between two BT datasets. The figure shows correlation performed for one position of the block (n x n). The resultant correlation coefficient returned value to the pixel marked in red. The dashed area on the BT correlation dataset contains pixels which are out of correlation coefficient determination because of their boundary position. 16

5 Calculation of correlation map. Letters C, D, E correspond to the intermediate product obtained during data processing (Figure 4). 17

6 Seasonal development of landfast ice in the southeastern Laptev Sea derived from ASAR imagery. Reprinted from Antonova (unpublished). 20

7 Correlation coefficients calculated with different Δ *days* between BT measurements: A 1 day; B 3 days; C 7 days; D 14 days. The white contours show the fast ice extent obtained from ASAR imagery (28 April 2008). 22

8 Correlation maps obtained with different *block size* parameter: A 3x3 pixels; B 5x5 pixels; C 7x7 pixels. For quality comparison, the white contours show the fast ice extent obtained from ASAR imagery (08 April 2008). 23

9 Correlation maps produced with different *block sizes* and *threshold* values. White contours show the fast ice extent obtained from ASAR imagery (08 April 2008). 24

10 Fast ice maps obtained for 14 November 2008 (A) and 26 January 2009 (B). White contours show the fast ice extent obtained from ASAR imagery for the same dates respectively. 26
11 Air temperature annual cycle base on Tiksi observatory records (2007-2011). The increase of air temperature which starts in March-April limits the algorithm application. 27

List of Tables

1 Validation data coverage 18
2 Standard parameters used for algorithm testing. 21

Glossary

AARI - Arctic and Antarctic Research Institute (St.Petersburg, Russia)

AMSR-E - Advanced Microwave Scanning Radiometer - Earth Observing System

ASAR - Advanced Synthetic Aperture Radar

AWI -Alfred Wegener Institute for Polar and Marine Research

BT -Brightness Temperature

ENVISAT -Environmental Satellite

GIS -Geographical Information System

MODIS -Moderate Resolution Imaging Spectroradiometer

NSIDC -National Snow and Ice Data Center

WMO -World Meteorological Organisation

SAR -Synthetic Aperture Radar

1 Introduction

1.1 Overview

Numerous definitions of landfast (fast ice, shore-fast ice) can be found in literature. The World Meteorological Organization (WMO) defines fast ice as sea ice which remains fast along the coast, where it is attached to the shore, to an ice wall, to an ice front, or over shoals, or between grounded icebergs. According to Flato and Brown (1996) landfast ice is a relatively immobile ice cover that has fastened along the coast or to the sea floor. The terms landfast and shore-fast ice point to its particular mechanism of attachment. However, in the literature fast ice, landfast ice and shore-fast ice are usually used as synonyms. Reviewing numerous definitions Mahoney et al (n.d.) indicated that all of them agree that fast ice is adjacent to the shore and characterized by a lack of motion. Fast ice is an important feature of Arctic and Antarctic coastal zones. However, there are strong hemispheric differences. In Antarctic grounded icebergs often serve as fast ice anchor points, which lead to fast ice occurrence in offshore territories with water depth of 400-500 m [Massom, 2001]. In a contrast, Arctic fast ice is a mostly a seasonal phenomenon; it starts to develop in autumn and breaks up in spring. The occurrence of multiyear landfast ice in the Arctic is limited to the Canadian Archipelago [Mahoney, 2007] and to parts of the Taymyr Peninsula [Reimnitz et al., 1995]. Arctic fast ice is typically grounded in shallow waters along the coast and at the shoals [Dmitrenko et al, 1999; Divine, 2004]. The variability in fast ice extent is a consequence of dynamic processes - attachment of ice floes and break-ups as well as thermodynamically ice formation and melting. The maximum extent of fast ice varies from tens to several hundred kilometers from the coast [Divine, 2004]. Figure 1 shows the fast ice extent in the Arctic for April 2010, when the fast ice extent is usually close to its maximum.

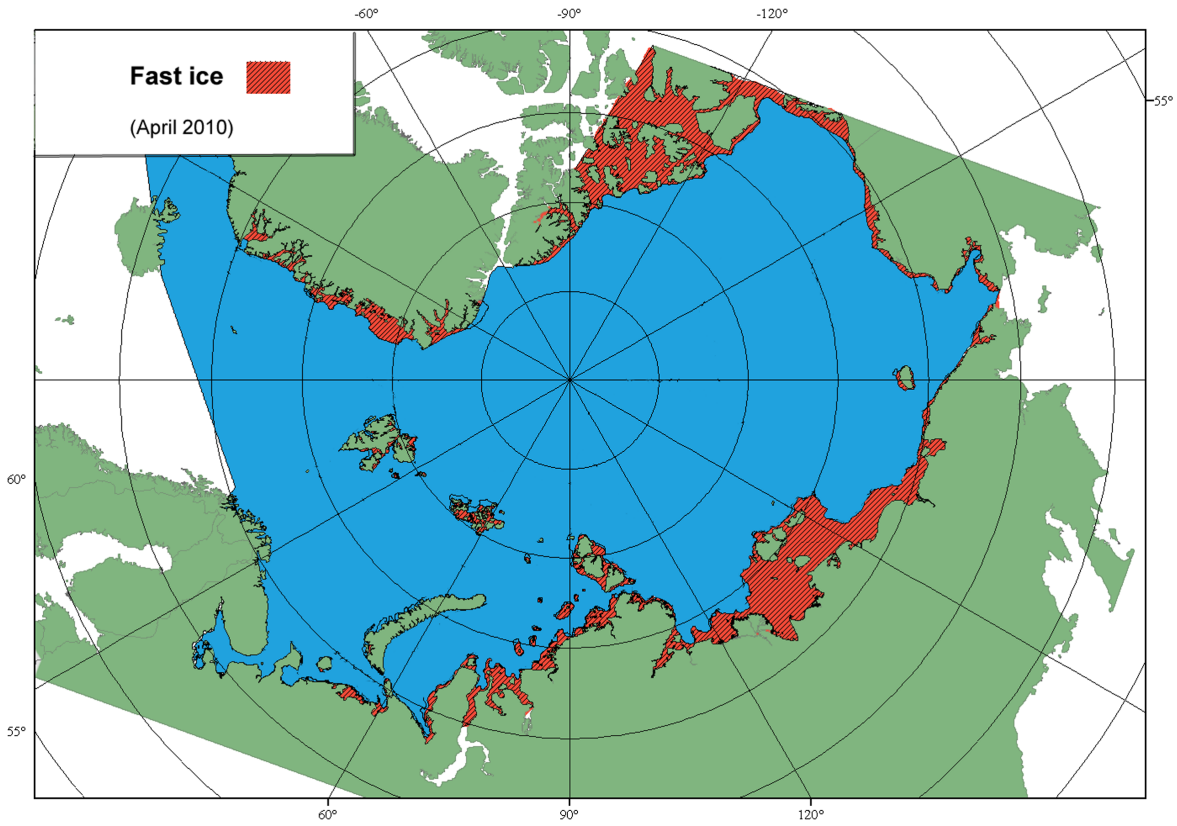

Figure 1: Fast ice extent for April 2010 (adopted from AARI, 2010).

Fast ice is important for various reasons: first, the location of the fast ice edge controls the position and shape of coastal polynyas. Coastal polynyas are ice free areas that develop when offshore winds drift the pack ice away from the fast ice edge. They are sites of strong ice production and ocean-to-atmosphere moisture and heat losses [Morales Maqueda et al., 2004]. Second, in the shallow zones and in the spits of the shelf seas, the presence of fast ice is important on helping to maintain submarine permafrost. It further offers protection from coastal erosion and thus controlling coastal morphology [Eicken, 2005]. Third, fast ice provides a habitat for micro-organisms and a hunting platform for large animals [Gjertz et al, 1986; Krell, 2003]. Moreover, the distribution of fast ice has significant implications for polar marine navigation and offshore exploration, particularly for the seas, situated along the North-East passage [Johannessen, 2005; Hughes, 2011]

1.2 Satellite based fast ice detection methods

Because fast ice remains fixed along the coastline it is possible to distinguish it from moving pack ice by means of remote sensing. Currently there are number of methods for detection and monitoring fast ice from space. The most common technique is based on distinguishing stationary and contiguous with the shore ice (which is assumed to be fast) from moving pack ice. The detection of sea ice is mostly based on correlation techniques on two consecutive satellite images [Kwok et al., 1998; Agnew et al. 1997]. Based on the type of used data the satellite based methods of fast ice detection can be broadly classified into three major groups:

-passive microwave based

-active microwave based

-visible/thermal infrared based

Visible/infrared data have relatively high spatial resolution from tens of meters to kilometers. However, the main disadvantage of this kind of observations is a strong dependence on weather conditions. Visible and infrared wavelengths are not able to penetrate clouds. Hence, clouds needs to be classified, masked and excluded from the image analysis before the fast ice detection procedure. Visible/infrared data from MODIS sensor was used for ice mapping for East-Antarctica region by Fraser et al. (2011). The study showed that the method required manual work and usage of additional data e.g. passive microwave based because of imperfect cloud masking. Active microwave based data has the highest spatial resolution of tens to 100s cm. An automatic technique for fast ice edge detection using Synthetic Aperture Radar(SAR) imagery was developed and tested for the Alaskan Arctic by Mahoney et al.(2004). However, an Arctic wide application is limited due to the low temporal and spatial coverage of this satellite product. Finally, passive microwave data is widely used for determining sea ice motion [Agnew et al., 1997, Kwok et al, 1998, Maslanik et al., 2004], but because of the low spatial resolution (5-50 km) it has not been used for fast ice mapping extensively [Fraser et al, 2011]. Nevertheless, the excellent spatial and temporal coverage and the ability to

penetrate clouds are the great advantages of passive microwave data.

1.3 Aim of this work

A drawback of current coupled sea ice-ocean models is the missing or deficient representation of fast ice. However, following Adams et al. (2010) and Rozman et al. (2011), a correct representation of the fast ice edge is important since it directly affects the accuracy of the model simulated sea ice drift, as well as the position and shape of polynya occurrence. The studies are based on comparisons between different model runs made with and without a generic fast ice masks and satellite observations. Since for most of the marginal seas of the Arctic Ocean, information on the seasonal variability and extent of the fast ice are not existent or strongly limited in time and space (see Chapter 1.2), the authors had to extract the shape and position of the immobile ice zone manually and limit the comparison to a single year. A permanent consideration of fast ice in coupled sea ice-ocean models would require an automatic procedure to derive fast ice extent for the entire Arctic at a reasonable spatial and temporal resolution. Aim of this thesis is therefore to investigate if brightness temperature data obtained from passive microwave satellites allows an automatic extraction of fast ice information. The presented method is based on a simple correlation technique, similar to the one used by Giles et al (2008) and Fraser et al. (2011). The implemented method was proposed by Prof. L. Kaleschke (pers. com.). In this thesis, the south-eastern Laptev Sea was chosen as the study area of interest, mainly because of the availability of a validation dataset. Moreover, the Laptev Sea fast ice extends as much as 400 km offshore [Dmitrenko et al., 1999] and shows great seasonal variability making it a suitable area to test performance and limitations of the presented technique. The thesis is structured as follows: Chapter 2 describes applied data and methods for automatic fast ice retrieval. Results are given in Chapter 3. Discussion of the results is presented in Chapter 4, while conclusions are drawn in Chapter 5.

2 Data and methods

2.1 AMSR-E data

In this work Advanced Microwave Scanning Radiometer (AMSR-E) brightness temperature information were used to map fast ice areas in the Laptev Sea. The AMSR-E is a twelve-channel, six-frequency, total power passive-microwave radiometer system. It measures brightness temperatures (BT) at 6.925, 10.65, 18.7, 23.8, 36.5, and 89.0 GHz. Vertically and horizontally polarized measurements are taken at all channels. The data were acquired from the National Snow and Ice Data Center (NSIDC) for the period from 2003 to 2011. In this study, vertically polarized BT data obtained from the 89 GHz-channel were used exclusively. As compared to other channels, the 89GHz channel has the highest spatial resolution (6.25 km) and is therefore most promising for an application in a fast ice detection procedure . However, unlike low frequency channels, BTs obtained at 89 GHz could be influenced by the presence of water vapor in the atmosphere [Spreen, 2007].

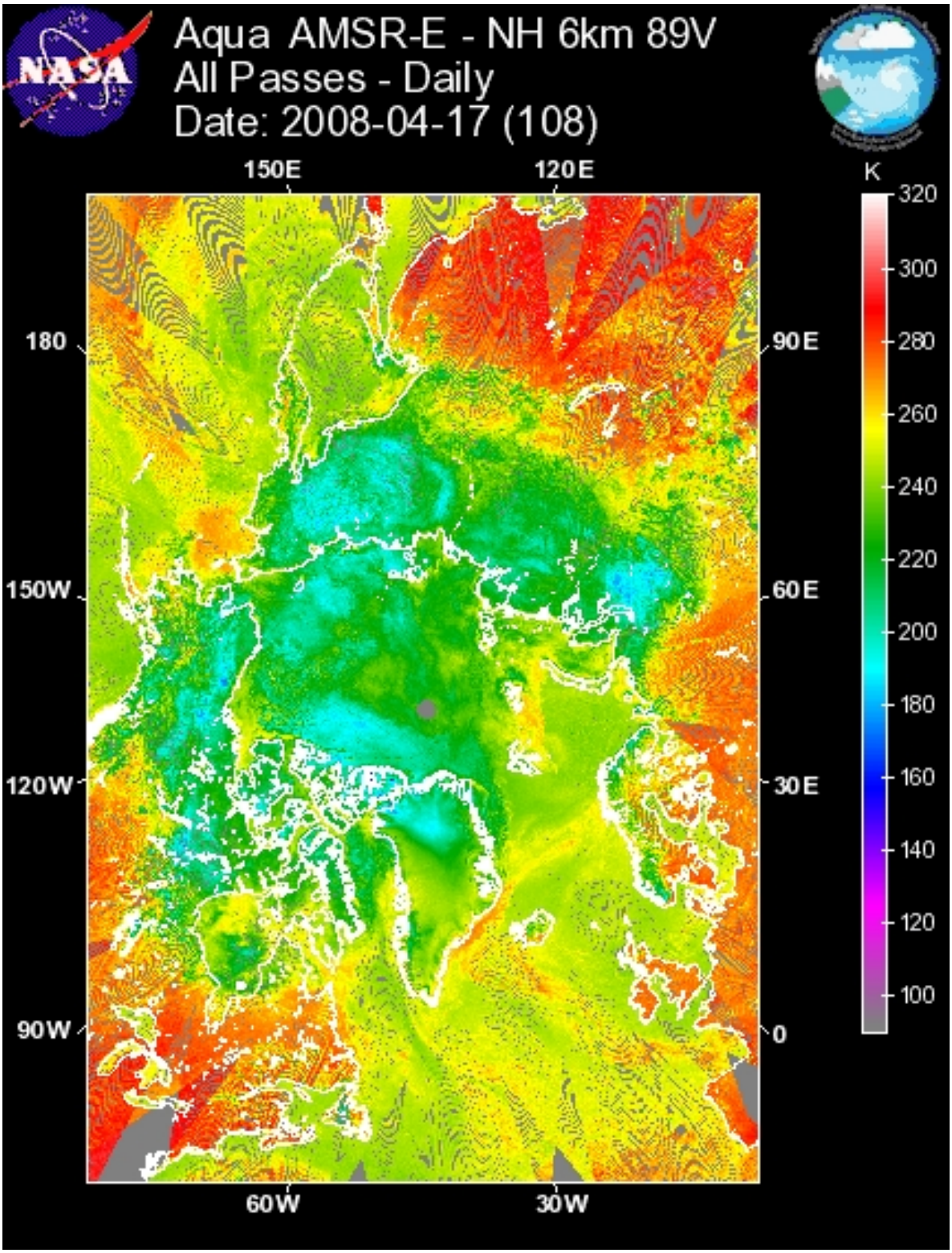

Figure 2: AMSR-E/Aqua daily average brightness temperatures from 89 GHz channel, vertically polarized. Grey colour indicates missing data.

2.2 Fast ice retrieval method

Brightness temperature measured by means of passive microwave sensors is a product of physical temperature and emissivity (emission coefficient) of the surface. In addition, the atmosphere has its contribution. The emissivity of a surface depends on its dielectric properties and its roughness. Neglecting the atmospheric influence, changes of BT in time show that physical properties of the surface (any combination of physical temperature, dielectric properties and roughness) have been changed. Correlation between two brightness temperature estimations reveals whether the surface has been changed during a certain time period or not. During winter BTs of fast ice and pack ice do not show any significant changes in time. Only at the onset of spring, BT characteristics undergo a dramatic decrease owing to changes in snow and ice structures (initiated by melting processes). The method that is used in this study to detect fast ice is based on a simple correlation technique between two consecutive images: Fast ice, that is fixed in space will show only little or no changes in BT. A correlation between image pairs will consequently result in a high correlation coefficiant over fast ice areas. In contrast, where ice is drifting, the BT is changing leading to a low correlation coefficiant (pack ice). Below the applied algorithm is described in detail (also see Figure 3).

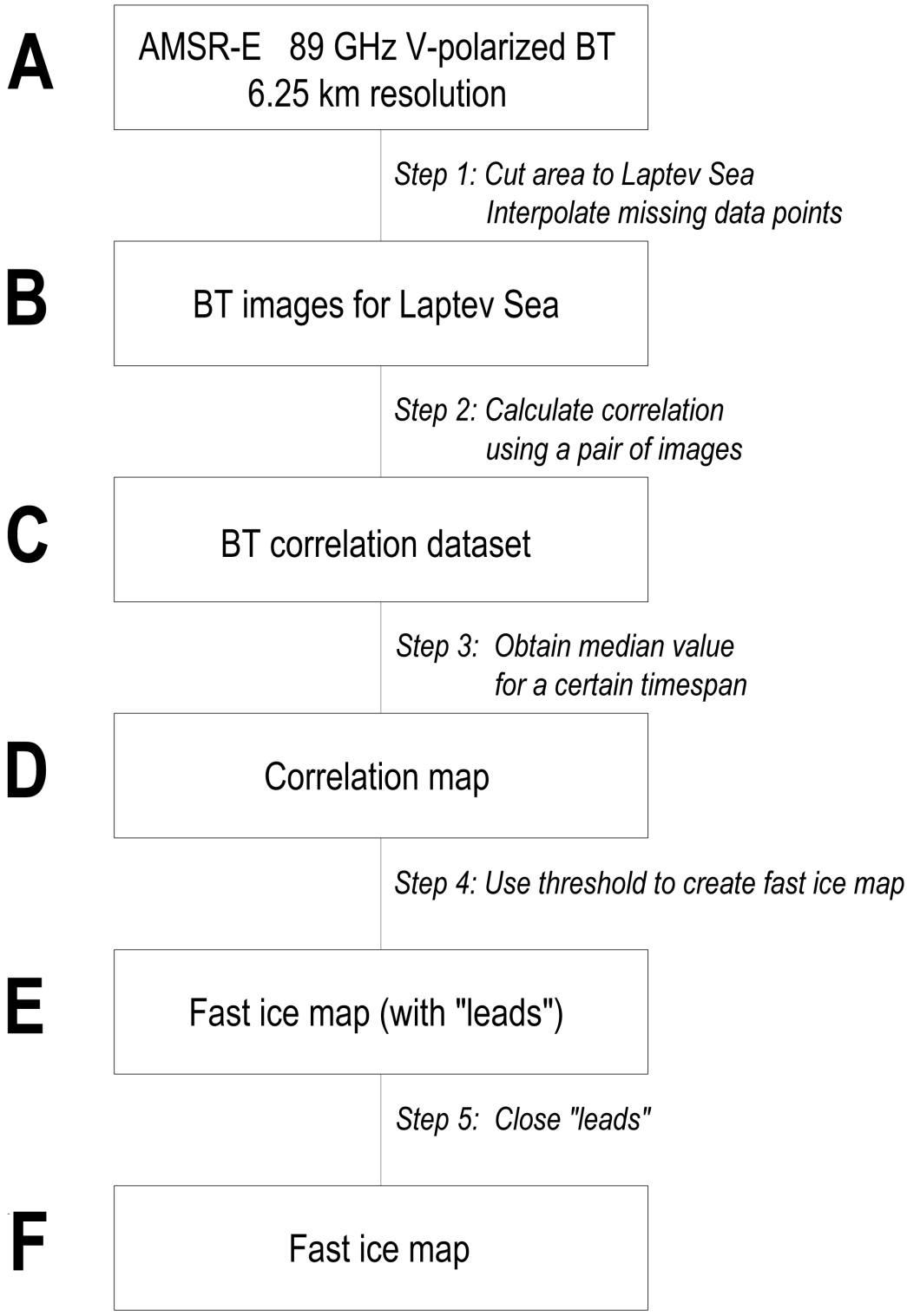

Figure 3: The flowchart shows steps of fast ice mapping. The letters refer to the kind of data obtained after each step.

Beforehand, areas that fall outside the Laptev Sea were excluded from processing and missing data were interpolated via the linear-interpolation method (Steps 1). Next, correlation was performed between two consecutive BT datasets. The time difference between the datasets (BT images) is referred to as Δ *days* hereafter. The correlation procedure (Step 3) is described below:

-both datasets were divided into small overlapping blocks of the same size (n x n), in such a way that each datapoint has a central position within one block. The exceptions were datapoints on the edge of the dataset which could not be central for a block.

-Pearson correlation coefficient between BT values comprising corresponding blocks within two datasets was calculated.

-the calculated correlation coefficient returned value for a pixel on the BT correlation dataset (Figure 4).

-a series of obtained BT correlation datasets, covering a period given by *time span* parameter were used to get median correlation coefficients (Figure 5). The number of BT correlation datasets used for obtaining one fast ice map equals the difference between time span and Δ *days*.

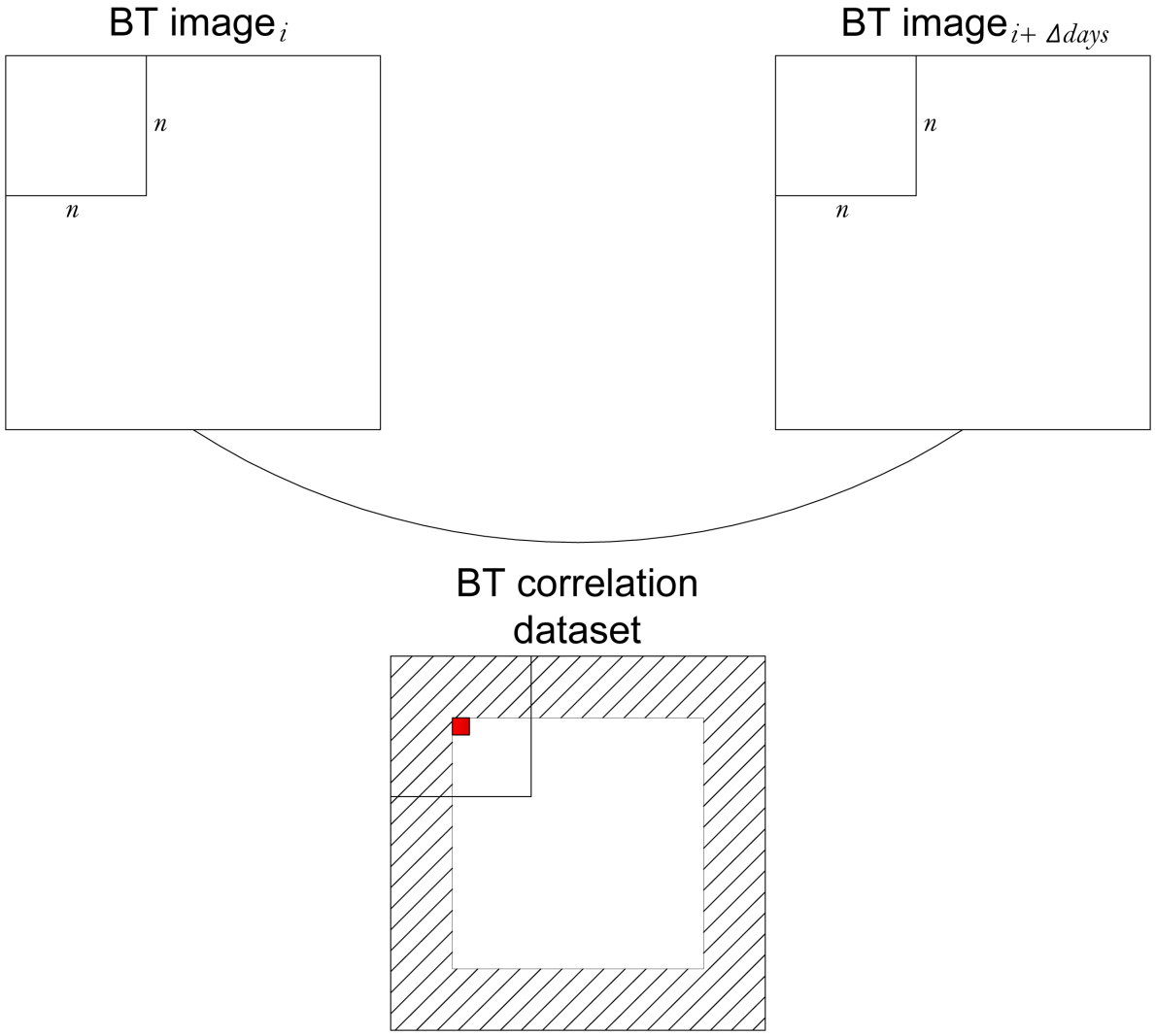

Figure 4: Calculation between two BT datasets. The figure shows correlation performed for one position of the block (n x n). The resultant correlation coefficient returned value to the pixel marked in red. The dashed area on the BT correlation dataset contains pixels which are out of correlation coefficient determination because of their boundary position.

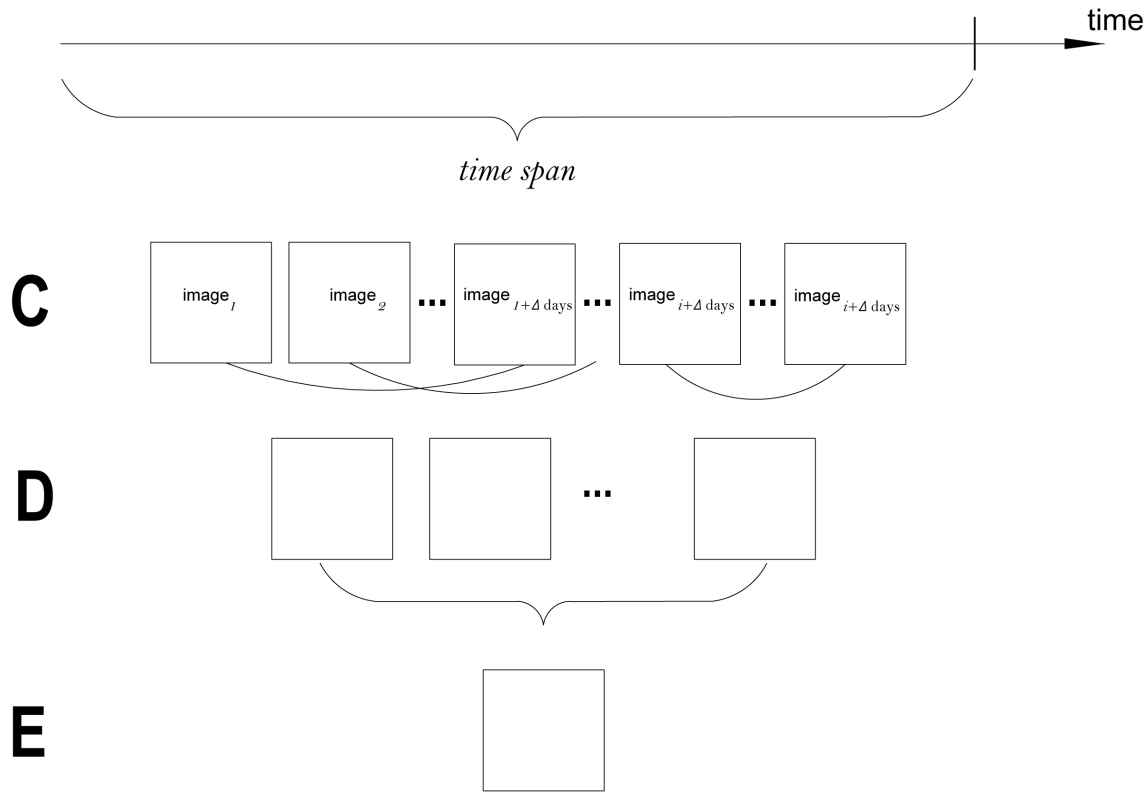

Figure 5: Calculation of correlation map. Letters C, D, E correspond to the intermediate product obtained during data processing (Figure 4).

Then the pixels of the correlation map characterizing by high correlation coefficients were treated as fast ice (Step 4). The minunum value of correlation coefficient, which characterize fast ice was difened by *threshold*. The resultan fast ice map had areas withing fast ice which wrongly were not classified as fast ice. In order to reduce this inacuracy, the procedurre of closing leads within fast ice areas was applied. The area covered by these lead were diminished by prescribing fast ice characteristic to the areas, completely surrounded by the fast ice in a radius of eight pixels. In Chapter 3 the method was applied and tested with different settings, namely changes in the algorithm parameters(Δ *days*, *time span*, *block size*, *threshold*) to optimize the algorithm results. The resultant fast ice mask is compared to the validation dataset, that is described below.

2.3 Validation dataset

For validation a high resolution fast ice product for the southeastern Laptev Sea area was used. The data were provided by the Alfred Wegener Institute for Polar and Marine Research (AWI). The product includes fast ice area and fast ice edge located by means of Environmental Satellite (ENVISAT) Advanced Synthetic Aperture Radar (ASAR) images. The applied ENVISAT C-band wide swath data is vertical-polarized and covers an area of approximately 400 800 km with a spatial resolution of 150 150 m. The fast ice edge was mapped manually based on analyzing two consecutive SAR images. Areas of freely floating pack ice and ice that appears to be without any drift were determined manually by toggling between image pairs. Areas fixed in space were then classified as fast ice. The clear boundary that exists between moving and stationary ice indicates the fast ice edge. The average time difference between image pairs is approximately 7 days. The fast ice area and edge location was stored in an ArcGIS shapefile. The validation dataset covers the time period from 2003 to 2011. Detailed information about temporal resolution of the dataset is contained in Table1. Reprinted from Antonova (unpublished).

Table 1: Validation data coverage

season/month	Nov	Dec	Jan	Feb	Mar	Apr	May	Jun
2003-2004	0	1	1	2	1	1	1	1
2004-2005	0	0	1	2	0	0	0	0
2005-2006	0	0	1	1	0	0	0	0
2006-2007	0	-	-	-	-	2	1	0
2007-2008	0	1	4	4	4	4	4	2
2008-2009	1	1	3	4	1	4	4	2
2009-2010	0	2	4	4	4	2	0	0
2010-2011	0	0	3	3	5	3	0	0

2.4 Pattern of seasonal fast ice development in the southeastern Laptev Sea

Fast ice in the Laptev Sea starts to develop in October [Rigor and Colony, 1997]. Figure 6 shows the monthly (December-June) development of the fast ice zone between 2003 and 2011. Typically the narrow fast ice band is already formed by the middle of December. At the same time spots of ice grounded at the shoals appear between the Novosibirskie islands and the continent. In the beginning of the season fast ice grows rapidly, and by the end of January the fast ice extent almost reaches its maximum. Further development goes on very slowly, without significant changes. Scarce data for the summer month shows that the extent close to the maximal is preserved at least until the end of June. By the beggining of August, most of waters are free of fast ice[Rigor, 1997]

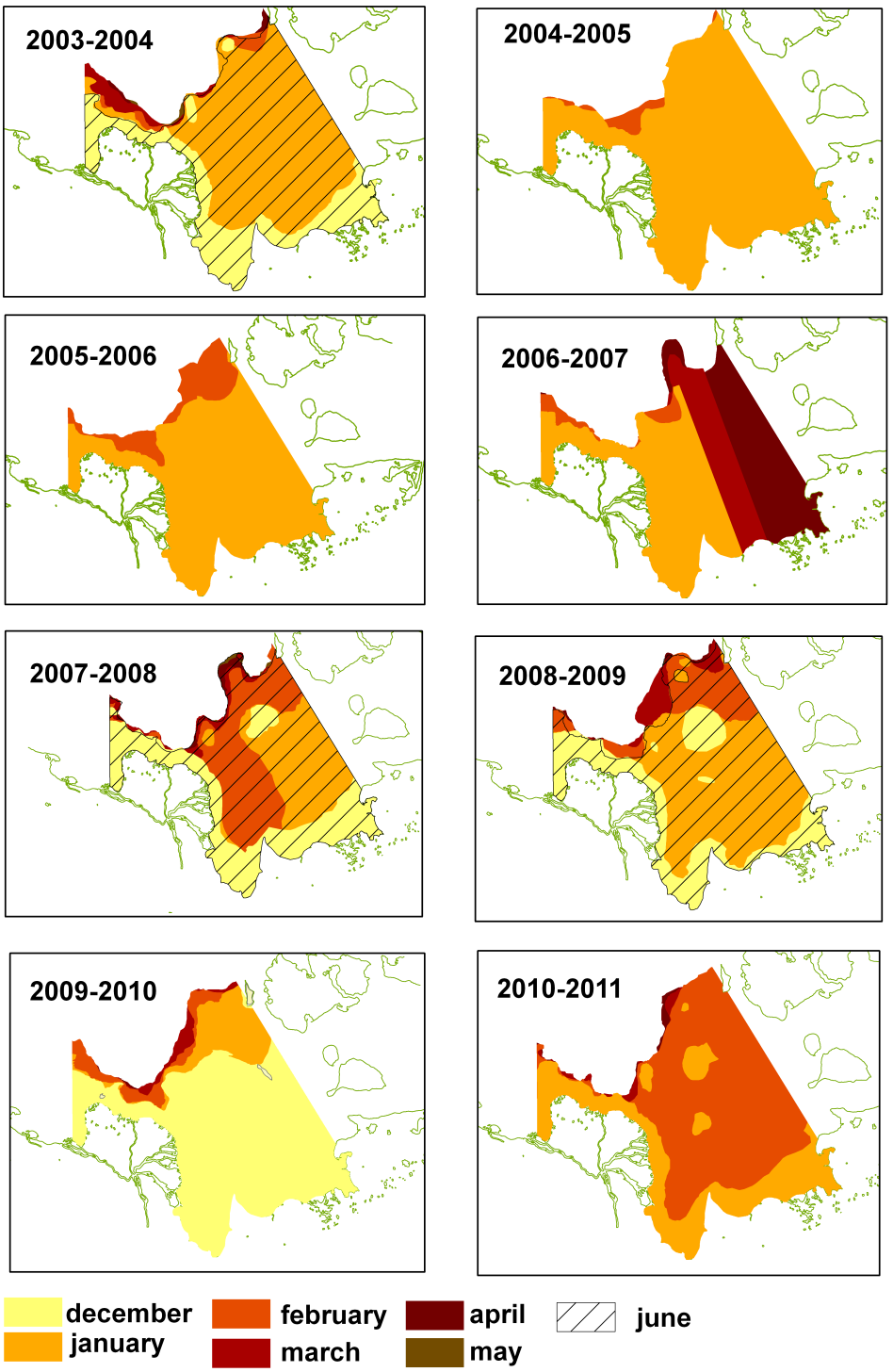

Figure 6: Seasonal development of landfast ice in the southeastern Laptev Sea derived from ASAR imagery. Reprinted from Antonova (unpublished).

3 Results

3.1 Assessment of the accuracy of the algorithm

The implemented in this study algorithm is based on four parameters: *block size*, Δ *days*, *time span* and *threshold*. Each of these parameters is essential for the quality of the results. Below, the impact of a changing *block size*, Δ *days*, *time span* and *threshold* is assessed separately, while the rest is set to a standard value, which turned out to be most promising for the presented approach.

Table 2: Standard parameters used for algorithm testing.

Parameters	standard values
block size	5×5
Δ days	7
time span	21
threshold	0.75

3.2 Impact of changing Δ *days* parameter

This parameter contains defines the time difference between two image pairs that were used for correlation. Taking into account that average sea ice drift velocity in the Laptev Sea does not exceed 5 km per 24 hours [Maslanik et al., 1998] and that the spatial resolution of AMSR-E data is 6.25 km, the time difference between images needs to be minimum 2 days. Figure 7 A demonstrates the effect of using different Δ *days* values for the retrieved correlation between two image pairs. If setting Δ *days* to 1, high correlation coefficients are characteristic for both fast ice and pack ice areas. A separation of fast ice areas from pack ice areas becomes impossible. The difference between pack ice and fast ice area becomes more pronounced with increasing Δ *days* (compare Figure 7 B, C). If setting Δ *days* to 3 or 7 days, correlation coefficients over fast ice area remain high, while the BT pattern over pack ice areas change, resulting

in low correlation coefficients. Only distinct pack ice areas are characterized by high coefficient. In general correlation coefficients for pack ice areas are lower, than for the fast ice. In a contrast, a too big time gap between correlated images is liable to expose low correlation coefficient over the fast ice (Figure 7 D). This is associated to changes in fast ice BT that occur on a time scale of several weeks. The reason for this change is not fully understood by now but might be related to changes in snow/ice structure and surface temperatures.

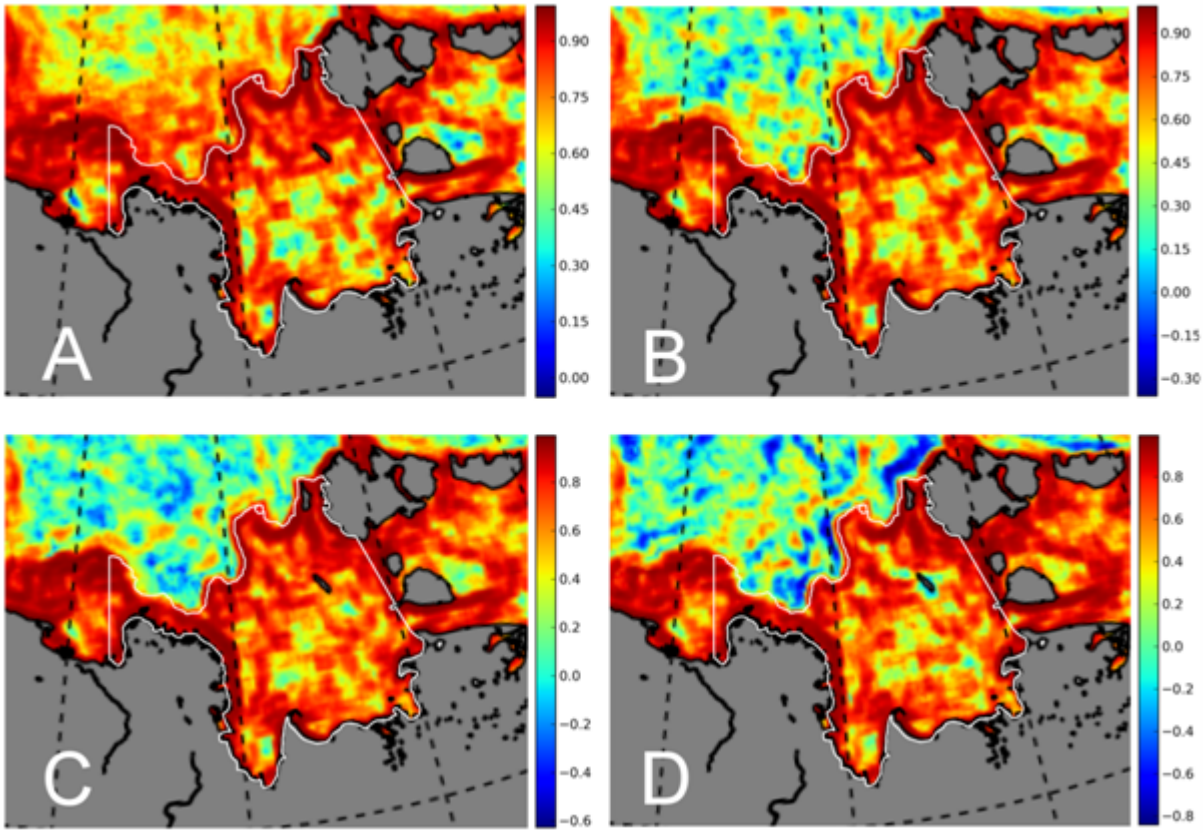

Figure 7: Correlation coefficients calculated with different Δ *days* between BT measurements: A 1 day; B 3 days; C 7 days; D 14 days. The white contours show the fast ice extent obtained from ASAR imagery (28 April 2008).

3.3 Impact of changing *time span* parameter

Time span together with Δ *days* define the number of BT correlation datasets which are used to obtain the correlation map (see Chapter 2.2). Therefore the obtained from the correlation map fast ice map shows a mean fast ice extent for of time determined by *time span* parameter. The varying *time span* does not result in significant changes in fast ice map.

3.4 Impact of changing *block size* parameter

As it was described in Chapter 2.2 already, the *block size* determined the number of dataset points which were used to compute a single correlation value. In other words, a block represents the certain area of the surface, which was analyzed for changes. Because of this the correlation maps obtained with different *block size*s reflect different spatial scales of surface changes. Figure 7 shows the correlation and fast ice maps obtained with varying *block sizes*.

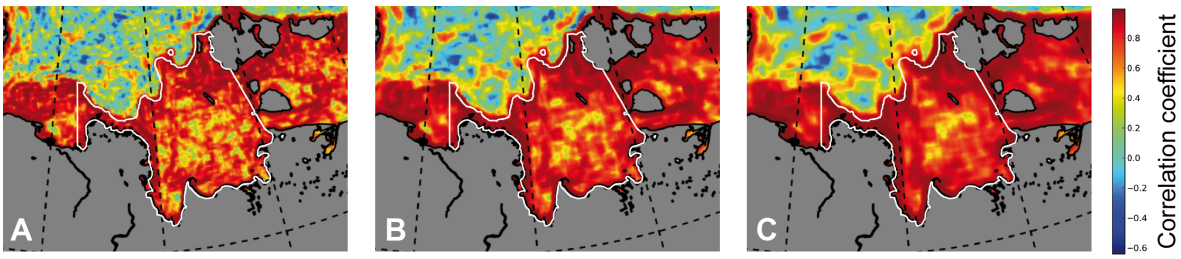

Figure 8: Correlation maps obtained with different *block size* parameter: A 3x3 pixels; B 5x5 pixels; C 7x7 pixels. For quality comparison, the white contours show the fast ice extent obtained from ASAR imagery (08 April 2008).

The smallest *block size* applied covers areas of 3 x 3 pixels (Figure 8 A), which is equivalent to an area of 19 km^2. On the correlation map the fast ice edge is well pronounced and shown by high correlation coefficients. However, the correlation coefficients within the center of the fast ice area are relatively low. This results in rather poor fast ice map quality (Figure 9 A 1-3).With increasing *block size* the changes in

BT appeared smoother, which results in more accurate mapping of fast ice area, but also more smoothed fast ice edge. Overall, the *block size* 5 x5 pixels was chosen as the standard parameter, which compromises between fast ice edge and area mapping accuracy.

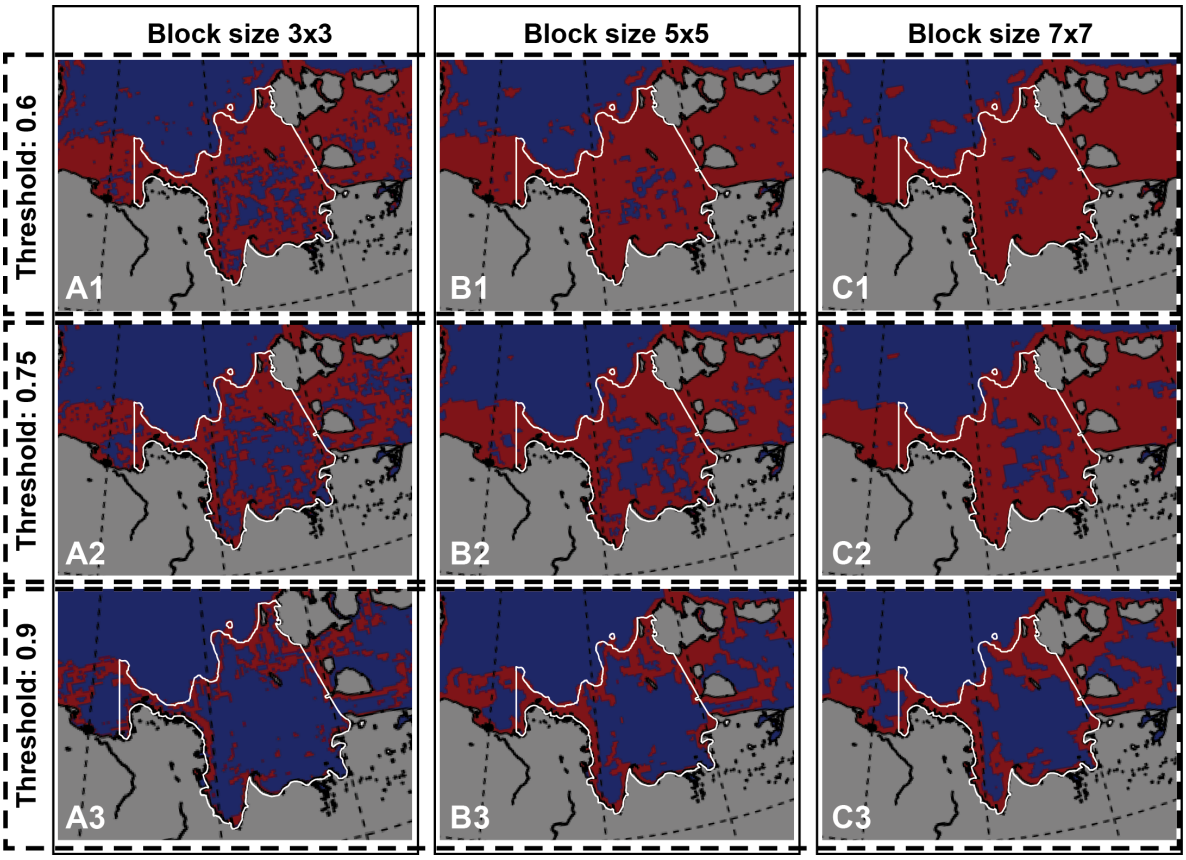

Figure 9: Correlation maps produced with different *block sizes* and *threshold* values. White contours show the fast ice extent obtained from ASAR imagery (08 April 2008).

3.5 Impact of changing *threshold* parameter

This parameter is important for final fast ice mapping. The choice of the *threshold* varies with the *block size*, v and *time span* that were used to generate the fast ice mask. (Figure 3, Steps 1-3). Usage of a high *threshold* values exclude pack ice areas from the final fast ice map that were misclassified as fast ice. However, a high *threshold*

also leads to a misclassification of fast ice areas that are located in the center of the fast ice zone. This is a consequence of changing BT values that may take place over this zone, in particular if using relatively high Δ *days* values. The way the *threshold* is set is therefore somewhat arbitrary and requires some tuning.

4 Discussion

AMSR-E 89 GHz brightness temperature observations were used for automatic mapping of landfast ice in the southeastern Laptev Sea. The implemented algorithm is based on a correlation technique similar to commonly used in satellite based methods of fast ice mapping [Fraser et al., 2011; Mahoney et al., 2004]. The algorithm was tested with different settings and the obtained results were compared with high resolution fast ice maps of the region. The obtained maps show a mean fast ice extent for a certain period of time determined by *time span* parameter (see Chapter 2.3). By using mean values the unbiased errors within the dataset are filtered out. It means that the possible errors induced for example by weather influence on the BT measurements are reduced. Validation reveals that the applied method maps fast ice edge rather accurate for the winter period (January-April). For this time period the position and curvature of fast ice edge mapped precisely (Figure 9 A1, B1). For the beginning of fast ice development (October-December) the algorithm gives less accurate results. However it is capable to detect enormous changes in fast ice extent, which take place in November-January (Figure 10).

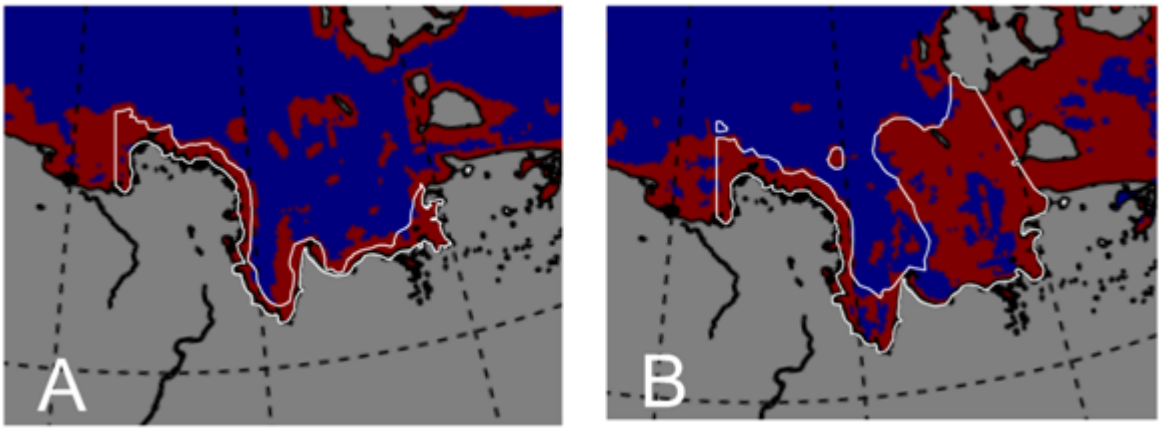

Figure 10: Fast ice maps obtained for 14 November 2008 (A) and 26 January 2009 (B). White contours show the fast ice extent obtained from ASAR imagery for the same dates respectively.

The method is not applicable for spring and summer period, which means that changes in fast ice extent during the break up period could not be revealed. Raising air temperatures in spring causes BT characteristics to change significantly, which gives low correlation coefficients over the whole fast ice area. The suitable application time period for the algorithm can be seen on annual air temperature cycle (Fugure 9).

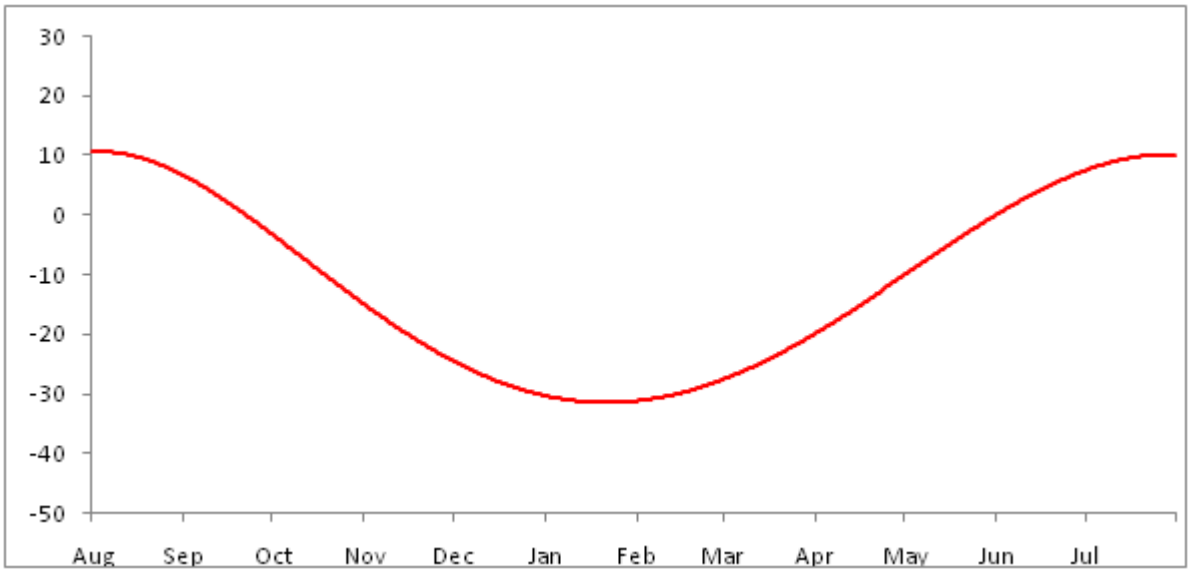

Figure 11: Air temperature annual cycle base on Tiksi observatory records (2007-2011). The increase of air temperature which starts in March-April limits the algorithm application.

The shortcomings of the algorithm are occurrence of spurious fast ice areas within pack ice zone as well as spurious leads within the fast ice. Some of these wrongly recognized fast ice zones can be removed by applying bathymetry data. Several studies link maximal fast ice extent with the bathymetry. Water depths cited as coinciding with the limit of landfast ice extent vary by location: 25 m along the Siberian coast [Zubov, 1945], 10 m in the Kara Sea [Divine et al., 2004], between 18 m and 30 m in the Beaufort Sea [Canadian Hydrographic Service, 1968; Kovacs and Mellor, 1974; Reimnitz and Barnes, 1974; Stringer, 1974; Shapiro, 1976; Kovacs, 1976; Weeks et al., 1977; Stringer et al., 1980], and 180 m off the eastern coast of Baffin Island [Jacobs et al., 1975]. [Mahoney et al., 2007]. Based on this knowledge bathymetric limitation for fast ice mapping can be used, however it will not affect the spurious fast ice areas which appear in vicinity of the fast ice edge. The bathymetry data were not used in this study and it can be seen as an possible later improvement of the algorithm. Some improvements also could be done in order to remove spurious leads. The procedure

of closing leads was used in the presented method of fast ice mapping. However, the applied simple algorithm is not able to close big leads.

5 Conclusion

This study presents a method for retrieving fast ice extent based on satellite passive microwave measurements, as well as the validation of this method. The technique uses daily BT measurements from AMSR-E 89GHz channel to distinguish fast ice from pack ice. The algorithm discriminates between fast ice and pack ice judging on level of surface changes during a certain time period. High level of surface changes is treated as pack ice zone characteristic. In a contrast, fast ice is distinguished by low surface changes. The fast ice maps were produced for the southeastern Laptev Sea. Next, the sensitivity of the presented method is evaluated with respect to changing algorithm parameters and compared to a validation dataset. The method is capable to reproduce the enormous fast ice changes that occur between November and January. The major disadvantage of the method is that its application is limited to a certain season (November-April for the southeastern Laptev Sea), since temperatures above freezing will substantially change BTs and hence making a reliable classification of pack and fast ice impossible. This study shows that the use of brightness temperature data obtained from passive microwave measurements offers great potential for an automatic fast ice mapping procedure to be used in coupled sea ice-ocean models. Nevertheless, further improvements (e.g. implementation of bathymetry data) are required to ensure a more reliable product.

Acknowledgement

I would like to thank my patient supervisors Ruediger Gerdes and Elena Shalina for the support and valuable comments. Many thanks go to Thomas Krumpen who contributed a great advisory support to this research. I would also like to express my special thanks to computer wizard Torben Klagge for both computer and moral support. In addition, I would like to thank Prof. L. Kaleschke whose courses I attended at Hamburg University. The knowledge I acquired there enabled me to choose this topic. I would also like to thank all the POMOR staff members and personally Dr. Heidemarie Kassens and Dr. Nadezda Kahro. Finally, I thank my friends and family who supported me enormously. This research was conducted in the frame of the BMBF-Projekt "POMOR - Deutsch-russischer Masterstudiengang fr angewandte Meeres- und Polarwissenschaften" (RUS 10/002). The financial support was provided by DAAD-Vorhaben "Stipendien Masterstudiengang fr angewandte Meeres- und Polarforschung POMOR vom 19.10.2009" (50733296) and Otto-Schmidt-Laboratory, Saint Petersburg.

References

AARI, Review ice charts of the Arctic Ocean [Online]. Available from: http://www.aari.ru/projects/ecimo/ (Accessed: 07 July 2011).

Adams, S., Willmes, S., Heinemann, G., Rozman,P., Timmermann R. and Schrder, D., 2011. Evaluation of simulated sea-ice concentrations from sea-ice/ocean models using satellite data and polynya classification methods. Polar research, Vol. 30.

Agnew, T. A., Le, H., and Hirose T., 1997. Estimation of large scale sea ice motion from SSM/I 85.5 GHz imagery, Ann. Glaciol., 25, 305 311 Antonova S., unpublished. Spatial and temporal variability of fast ice in the Russian Arctic. Thesis, (MSc). Saint Petersburg State University, University of Hamburg

Cavalieri, Donald, Thorsten Markus, and Josefino Comiso. 2004, updated daily. AMSR-E/Aqua Daily L3 6.5 km Brightness Temperature, Sea Ice Conentration, Snow Depth Polar Grids V002, [2007-2011]. Boulder, Colorado USA: National Snow and Ice Data Center. Digital media. Available from:

Dmitrenko, I. A., Gribanov, V. A., Volkov, D. L., Kassens H, and Eiken, H, 1999. Impact of river discharge on the fast ice extension in the Russian Arctic shelf area. Proceeding of the 15th International Conference on Port and Ocean Engineering under Arctic Conditions (POAC99), Helsinki, 23-27 August, Tech. Rep. 1.

Eicken H., Dmitrenko, I. A., Tyshko, K., Darovskikh, A., Dierking, W., Blahak, U., Groves, J., and Kassens H. Zonation of the Laptev Sea landfast ice cover and its importance in a frozen estuary. Global and Planetary Change, vol. 48, pp. 5583, 2005

Flato, G. M. and Brown, R.D. 1996. Variability and climate sensitivity of landfast Arctic sea ice. Journal of Geophisical Research, vol. 101, no C10, pp.257676-25777.

Fraser, A.D., 2011. East Antarctic landfast sea-ice distribution and variability. Thesis, (PhD). Institute for Marine and Antarctic Studies, University of Tasmania.

Fraser, A.D., Massom, R.A., Michael, K.J., 2011 Generation of high-resolution East Antarctic landfast sea-ice maps from cloud-free MODIS satellite composite imagery. Remote Sensing of Environment.

Gjertz and Lydersen, C., 1986. Polar bear predation on ringed seals in the fast-ice of Hornsund, Svalbard. Polar Research, vol. 4, pp. 6568.

Hughes N., Wilkinson, J. and Wadhamns P., 2011. Multi-satellite sensor analysis of fast-ice development in the Norske er Ice Barrier, northeast Greenland. Annals of Glaciology, vol. 52, no. 57, 2011.

Johannessen, O. M., Alexandrov, Yu, I., Frolov, Y., Sandven, S., Miles, M., Bobylev, L. P., Pettersson, L. H, Smirnov, V. G., and. Mironov, E. U, 2005. Remote Sensing of Sea Ice in the Northern Sea Route: Studies and Applications. Springer Praxis Books.

Kattner, G., Naumov, A., Evans, D., Dieckmann, G. and Thomas, D., 2003.The biology and chemistry of land fast ice in the White Sea, RussiaA comparison of winter and spring conditions. Polar Biology, vol. 26, no. 11, pp. 707719.

Kwok, R., Schweiger, A., Rothrock, D.A. Pang, S. and Kottmeier, C., 1998. Sea ice motion from satellite passive microwave imagery assessed with ERS SAR and buoy motions, J. Geophys. Res., 103, 8191 8214.

Mahoney, A., Eicken, H., Graves, A., Shapiro, L., 2007. Alaska landfast sea ice: Links with bathymetry and atmospheric circulation. JOURNAL OF GEOPHYSICAL RESEARCH, VOL. 112, C02001, doi:10.1029/2006JC003559.

Mahoney, A., Eicken, H., Graves, A., Shapiro, L., and Cotter, P., 2004. Landfast sea ice extent and variability in the Alaskan Arctic derived from SAR imagery. IEEE International Geoscience and Remote Sensing Symposium Proceedings, Vol. 3. (pp. 21462149).

Mahoney, A., Eicken, H., Shapiro, L., and Graves, A, n.d. Mapping and Characterization of Recurring Spring Leads and Landfast ice in the Beaufort and Chukchi. Project documentation [Online]. Available from: http://mms.gina.alaska.edu/supp/Definition.pdf (Accessed: 05 June 2011)

Maslanik, J., Agnew, T., Drinkwater, M., Emery, W., Fowler, C., Kwok, R., et al., 1998. Summary of ice-motion mapping using passive microwave data. Tech. rep., National Snow and Ice Data Centre, report prepared for the NSIDC at the request of the NSIDC Polar Data Advisory Group.

Massom, R. A., Hill K. L., Lytle V. I., Worby, A.P., Paget, M.J., and Allison I., 2001: Effect of regional fast-ice and iceberg distributions on the behavior of the Mertz Glacier polynya, East Antarctica. Annals of Glaciology, 33, 391-398.

Morales Maqueda, Willmott, M.A., A.J., and Biggs, N.R.T., 2004. Polynya dynamics: a review of observations and modeling. Rev.Geophys., 42(1), RG1004.

Rigor, I., Colony, R., 1997. Sea-ice production and transport of pollutants in the Laptev Sea, 1979-1993. The Science of the Total Environment 202 (1997) 89-110.

Reimnitz, E., Eicken, H. and Martin, T., 1995. Multi-year fast ice along the Taymyr peninsula, Siberia, Arctic, 48, 359367.

Rozman, P., Hlemann, E., A., Krumpen, T., Gerdes,R., Kberle,C., Lavergne,T., Adams S. and Girard-Ardhuin, F, 2011. Validating satellite derived and modelled sea-ice drift in the Laptev Sea with in situ measurements from the winter of 2007/2008. Polar Research, Vol 30.

Spreen, G., Kaleschke, L., Heygster, G., 2008. Sea ice remote sensing using AMSR-E 89 GHz channels. Journal of Geophisical Research

World Meterological Organization, 1970, WMO sea-ice nomenclature. Terminology, codes and illustrated glossary. WMO/OMM.BMO No. 259, 145 pp, Geneva Secretariat of the World Meteoroligical